Signal extraction of cosmic string topological defects

Jeffrey Morais[a]

[a] *Department of Physics, McGill University, Montréal, Québec, Canada*

E-mail: jeffrey.morais@mail.mcgill.ca

Abstract: Topological singularities occurring in the parameter space of fields modify their observables and leave non-decaying signals in the spacetime they are defined over. These signals can occur at high energy scales and so are of interest for probing the formation structure of the universe. We investigate classes of quantum field theories which admit these topological defects and describe their stability via constraints on the homotopy classes of the fields' symmetry groups. In particular, we consider the case of a principal U(1)-bundle which gives rise to linear defects known as *cosmic strings* that occur in a phase transition in the early universe via the Kibble-Zurek mechanism. To isolate the cosmic string signal in 21cm observations we look for detecting the temperature gradient left in its wake, which is obscured by ΛCDM cosmological perturbations. We present a procedure to enhance and isolate the signal of the string from ambient primordial noise using match filtering statistics. It is found in the regime where the tension of the string is $G\mu \sim 3 \times 10^{-7}$ that a 1D unfolded match filter of the temperature matrix shows a clear indication for what the string signal looks like immersed in noise. We also demonstrate the domain in which the string signal is bounded by.

Contents

1 Introduction

It is of interest in theoretical physics to study the structure of the universe at different energy scales. One way to probe this information would be to consider the *topology* of its spacetime manifold from which we can constrain the fields defined on it, as well as the submanifolds it admits, via its cohomology and homology groups, respectively[†]. Additionally, one could consider its topological invariants which remain unchanged under continuous deformations of the space, such as the manifold's Betty/Hodge numbers and their associated Euler characteristic, which allow us to count how many fields are defined on the spacetime. Of the invariants which persist after deformation, one of particular interest are topological *defects* or *singularities* that occur whenever there is a discrepancy between boundary conditions on a cycle due to multiple homotopically distinct solutions of a some differential equation [1]. In the context of quantum field theory, these occur in the vacuum structure due to spontaneous symmetry breaking and come from inflationary phase transitions in the

[†]Given the forms in the cohomology group, we can recover the fields defined over the spacetime given a *flat musical isomorphism* $\sharp$ which maps between the cotangent and tangent bundles.

early universe. Being that it persists with time, this would allow us to study the formation structure of the universe long after the transition. The vacuum structure is formed as a quotient space between the gauge group G of the gauge theory and its subgroup H, and is known as the *moduli space* of vacua or the *vacuum manifold*. The vacuum manifold itself immersed in the parameter spaces of the fields defined over the spacetime and the defect modifies the observables of said field. Formally, defects are discontinuous functions that map from the spacetime to the vacuum manifold and are characterized by their codimension. These defects are presented with rigorous foundations in topological quantum field theory with the use of category theory [2]. The presence of these defects leads to observable signals in spacetime, and to study the formation structure of the early universe these signals must be extracted from ambient fluctuations which obscures them.

Consider for example a non-Abelian gauge theory with some G-bundle over the spacetime manifold $\mathcal{M}$, which is endowed with a natural connection $A = A^a_\mu \otimes dx^\mu \otimes t_a$. Here A^a_μ are the components of the connection where the indices a run over the generators of the gauge group G while μ labels the different points in $\mathcal{M}$, dx^μ is the basis of the associated cotangent bundle $T^*\mathcal{M}$, and t_a are the generators of G. The dynamics of the gauge theory are given by the Yang-Mills action, but for the sake of discussing topological defects from symmetry breaking we will couple the theory to fermionic spinors and massless scalars. The action of such is given by [3]:

$$S = -\frac{1}{2}\int \mathrm{tr}(F \wedge \star F) + \int d^4y \left[\frac{1}{2}(D\phi)^2 + \bar{\psi}(i\not{D} - m)\psi - V[A, \phi; g] \right] \tag{1.1}$$

The first term is the gauge invariant second Chern form [4] which describe the dynamics of the gauge field, where $F = dA + A \wedge A$ is the curvature 2-form of $\mathcal{M}$. The second term describes the dynamics and coupling of the fermionic and scalar fields, where $D\phi = d\phi + A \wedge \phi$ is the exterior covariant derivative acting on a massless scalar field ϕ, $\not{D}$ is shorthand notation for a contraction with gamma matrices, ψ is a complex spinor field of mass m, and $V[A, \phi; g]$ is a potential functional of interacting terms for some coupling constant g. Notice the lack of spinor terms in the potential functional as that would make the interaction vertex non-renormalizable. The action admits phase symmetries due to its invariance under local transformations on the spinor and scalar fields, respectively given by:

$$\psi \longrightarrow \exp\left(i\alpha^a t_a\right)\psi, \quad \phi \longrightarrow e^{i\beta}\phi, \tag{1.2}$$

where α^a are complex coefficients contracted with the generators, and β is some integer. For a fixed energy scale, the scalar symmetry maybe be spontaneously broken via a phase transition which occurs when cooling down the system past a critical temperature. The scalar field ϕ is defined to be the symmetry breaking parameter and has an associated potential $V(\phi) \subset V[A, \phi]$ which is independent of the other fields. The structure of the potential is altered during the phase transition which usually occurs in the form of the decay of a false vacuum via bubble nucleation. The vacuum manifold M of the scalar field is defined as the minimum domain of the potential given by $M \coloneqq \min_\phi V(\phi)$, and

irregularities of boundary conditions on M is what leads to the formation of topological defects (and their associated signals). These defects have specific conditions for stability which is characterized by homotopy classes of the symmetry group G. For the case where the defects developed from phase transitions in the early universe, these signals allows us to learn about the formation structure of the universe during early periods in its development. The search for this signal becomes difficult when it is obscured by primordial noise coming from cosmological perturbations. Specifically, we are interested in the case where the symmetry group is $G = U(1)$ and so the defects associated with a principal $U(1)$-bundle are 1-dimensional *cosmic strings*. These are useful as their mass energy density is proportional to the symmetry-breaking energy scale and thus allows us to probe the structure at very high energy scales in the early universe. In this case the noise which veils the signal comes from cold dark matter perturbations in the ΛCDM model. In this paper we develop what the cosmic string signal looks like in spacetime and develop statistics for extracting its signal amidst the non-linear noise in 21cm observations.

2 Stability constraints of topological defects

Topological defects persist under continuous deformations of the manifold given certain constraints of their homotopy groups. Such constraints are characterized by sequences of injective maps which describe the symmetry breaking patterns associated with phase transitions that create the defects. Additionally this gives us information on the stability of the defect in a given quantum field theory which allow us to see what defects form after a phase transition in the early universe.

2.1 Deformation classes via homotopy groups

To classify different topological defects, we must look at classes of topological space subsets which are equivalent to each other under continuous deformations. These are are described precisely with *homotopy* groups which are sequences of groups that generalize the fundamental group and record the topological information of the space. Additionally, if these topological spaces are locally isomorphic to Euclidean space, and the transition functions between its open subsets are smooth, they become manifolds. As an example of studying the topology of a manifold via its homotopy group consider a 3-dimensional cycle which cannot be trivially deformed into a point. This points to the existence of a singularity and thus the manifold admits a non-trivial genus. These properties can be additionally explored with height functions in Morse theory but for our purposes we stick to homotopy classifications.

Depending on the system, one can have multiple phase transitions which lead to multiple topological defects that depend on the information of the previously formed ones. These are known as *composite* defects and are characterized by sequences of symmetry breaking. Defects occurring only after one symmetry break are known as *singular* defects. Let's start by considering a symmetry breaking pattern in which the underlying symmetry group G reduces to a subgroup of itself H (usually its isotropy subgroup), which then breaks to another subgroup and so forth. This is denoted by the following:

$$G \longrightarrow H \longrightarrow \dots \tag{2.1}$$

One finds such a symmetry breaking pattern in the Georgi-Glashow model [5], a proposed model for a grand unified theory, in which the unified gauge group $SU(5)$ spontaneously breaks into the symmetry group of the Standard Model:

$$SU(5) \longrightarrow SU(3) \times SU(2) \times U(1). \tag{2.2}$$

During each step in the symmetry breaking pattern, we must verify stability conditions on the defect to see whether or not the gauge theory admits them. To do so we define a homeomorphism between the vacuum manifold M and its quotient space representation G/H, written as $M \simeq G/H$. Formally, this can be understood as the set of all equivalence classes of G, where two elements of a class differ by an element of H. In other words, elements $g \in G$ are mapped to the left cosets of H in G, given by $\{gh\}$ where $h \in H$ [4]. Thereafter, we look at the homotopy groups which characterize the topology of M. Consider for example an equivalence class of maps which send points from an n-sphere S^n to M, under the condition that a base point is preserved in the mapping. The equivalence class of these maps are known as *homotopy classes*. Two maps f_1, f_2 within this class are homotopically equivalent if they can be continuously deformed into one another via a continuous 1-parameter family of maps $f(t)$ which adhere to the conditions given by [6]:

$$f(t) : S^n \to M \mid t \in [0,1],\ f(0) = f_1,\ f(1) = f_2 \tag{2.3}$$

The homotopy classes form a group structure known as the *n-th homotopy group*[†] of the vacuum manifold M, denoted $\pi_n(M)$, which is the set of all homotopy classes of maps $f_k : S^n \to M$ [7] for $k \in \mathbb{Z}$. The first homotopy group $\pi_1(M)$ is known as the *fundamental* group of a manifold, and is the group of equivalence classes under homotopy of loops within M; that is to say the set of loops that can be continuously deformed into each other given a 1-parameter family of maps. The non-triviality of this group gives rise to 1D line defects known as *cosmic strings*. Furthermore, the second homotopy group $\pi_2(M)$ is the group of homotopy classes of closed 2-dimensional surfaces in M [8]. The non-triviality of this group gives rises to 0D defects known as *monopoles*. This intuition can be extended for all $n \geq 1$, which include defects such as 2D *domain wall* defects and 3D *texture* defects. These topological defects can occur in quantum field theories such as the Wess-Zumino-Witten model [9, 10] — a 2D conformal field theory used to describe superstring theory on $AdS_3 \times S^3$ — which appear on the worldsheet of physical strings. We now move on to describing the stability of these topological defects based on constraints of their homotopy groups.

2.2 Symmetry breaking as exact sequences

A theory admits a local/global *topologically stable* defect if the homotopy group is non-trivial, meaning (for the case of the vacuum manifold M) it obeys the condition [11]:

[†]It is noted that $\pi_n(M)$ is a group only for $n \geq 1$ and $\pi_0(M)$ is only a set.

$$\pi_n(M) \neq \mathbb{1},\ n \in \mathbb{Z}. \tag{2.4}$$

In general, stability conditions are often more intricate than the statement above such as for composite defects which deal with both the nature of the vacuum manifold, and the symmetry group G.[‡] The computations of these conditions on the homotopy groups are derived efficiently from sequences of injective maps, known as *exact sequences*.

Consider a pair of maps $f : A \to B$, $g : B \to C$ which map between manifolds A, B, C. The sequence $A \to B \to C$ coming from the map $g \circ f$ is *exact* if and only if the image of f coincides with the kernel of g. This is visualized in the following figure:

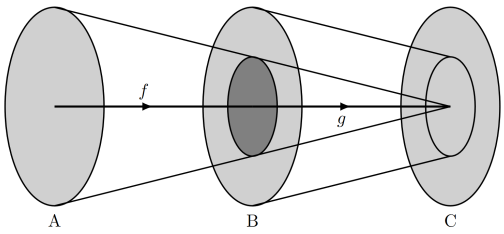

Figure 1. Visualization of an exact sequence of functions mapping between various manifolds. The shaded region within the manifold B represents the image of f, as well as the kernel of g [11].

For consideration of composite defects, we can consider a longer sequence of maps that are exact at every intermediate point. To describe such for the vacuum manifold, consider an injection map i from the homotopy group of H to the homotopy group of G and a projective map p from the homotopy group of G to the homotopy group of $M \simeq G/H$. These are defined respectively as:

$$\begin{aligned} i &: \pi_n(H) \to \pi_n(G) \\ p &: \pi_n(G) \to \pi_n(G/H). \end{aligned} \tag{2.5}$$

This gives us a set of n-corresponding maps for our large exact sequence between homotopy groups of the same degree n. We can further this by including sequences that map between homotopy groups of different degrees via *lifting* homotopy group elements. To do so, consider a fibre bundle composed of a base space G over the projected space G/H. We can lift an element of $\pi_1(G/H)$ — a loop — living in G/H to a loop in G, and being that the loop in the projected space returns to a starting point, the curve must end at an element of $H \subset G$ in the base space (which is true unless it admits a non-trivial holonomy or geometric phase). This might seem unintuitive, but one could think of it in reverse: if we identify the two endpoints of the curve in H via the modulo of G with H, the two endpoints become the same point in G/H and so the curve must return to its starting point. This is similar in principle to identifying the endpoints of a line to recover a circle

[‡]In this paper all symmetry groups are taken to be Lie groups, thus they are also endowed with the structure of a manifold.

which is done via a similar modulo map. The lift of a curve in the projected space to the base space is visualized in the following figure:

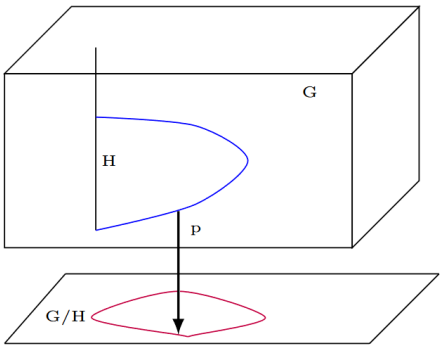

Figure 2. Lifting a loop (red) from the projected space G/H to a curve (blue) in the base space G via the inverse of the projective map p [11]. This can be seen as undoing the identification of the starting and end points of the loop in G/H to give two separate points in G which end on H.

Moreover, if the final element of the curve in H belongs to the same component as the identity in G, we can deform it continuously until the endpoints are themselves the identity and the curve forms a loop in G. Each homotopy class of loops in G/H defines a component of H, and in general we can define the lifting map ∂ between the homotopy group of G/H to the homotopy group of H of one degree lower as:

$$\partial : \pi_n(G/H) \to \pi_{n-1}(H) \tag{2.6}$$

This gives us a map that sends homotopy groups to ones of a different degree. Using the maps we defined to go between homotopy groups of different/same degrees, we can construct a long exact sequence of alternating maps which terminates at the lowest degree homotopy group $\pi_0(G/H)$. This is represented in the following:

$$\begin{aligned} \cdots \longrightarrow \pi_2(G) \longrightarrow \pi_2(G/H) \longrightarrow \pi_1(H) \longrightarrow \pi_1(G) \longrightarrow \\ \pi_1(G/H) \longrightarrow \pi_0(H) \longrightarrow \pi_0(G) \longrightarrow \pi_0(G/H) \end{aligned} \tag{2.7}$$

How exactly does this exact sequence between different homotopy groups help us recover stability conditions of topological defects? Using the requirement that the phase transitions must form an exact sequence, we can impose certain conditions to reduce the sequence to give us relations between homotopy groups [11]. These shortened exact sequences gives us the precise relations to tell us if the topological defect associated with the homotopy group is stable. Following this, we present some stability conditions for a few defects.

For a Lie group G which itself also has the structure of a manifold, it turns out that the second homotopy group is always trivial, i.e. $\pi_2(G) = \mathbb{1}$. This means that the group manifold itself will not admit defects such as monopoles. If the fundamental group of G is non-trivial, meaning G is simply connected, we can replace G by its universal covering group $\tilde{G}$. Finally, from the conditions previously mentioned, if we have a sequence structure

that looks like $\mathbb{1} \to A \to B \to \mathbb{1}$ then it follows that A and B are isomorphic ($A \simeq B$), and the sequence reduces to the equivalence [11]:

$$\pi_2(G/H) = \pi_1(\tilde{H}) \tag{2.8}$$

The above is the stability condition for a monopole, and states that the theory admits topologically stable monopoles in the vacuum manifold $G/H \simeq M$ if and only if the universal covering of the subgroup H is non-simply connected. Furthermore, if we restrict G to its connected part G_0 and define the connected part of the subgroup $H_0 = H \cap G_0$, then sequence reduces to the equivalence:

$$\pi_1(G/H) = \pi_0(\tilde{H}_0) \tag{2.9}$$

The above is the stability condition for a cosmic string, and states that topologically stable cosmic strings exist in M if and only if $\tilde{H}_0$ has disconnected pieces. Thus in our search for the cosmic string signal amidst the cosmological perturbation, we impose the relation on symmetry groups we work with (in particular when $G = U(1)$) to ensure their stability. Similar stability conditions may be derived for higher dimensional topological defects — such as domain walls or textures — with conditions on their higher degree homotopy groups. It is noted that for the stability conditions of composite defects, *relative* homotopy groups are used such as $\pi_n(M, M')$ where M' has identical properties to M. We now turn our attention specifically to cosmic string topological defects as they allow us to probe the universe structure at very high energy scales. We begin by describing the formation of cosmic strings from a specific scalar field symmetry breaking potential $V(\phi)$ in the proceeding section.

3 Cosmic string defects

In this section we delve into the formulation of the cosmic string line defects which allow us to probe the formation structure of the early universe at very high energy scales. We begin with describing how they form via spontaneous symmetry breaking and follow with some constraints on their properties such as how they can form loops. Finally, we look at their signal in spacetime which takes the form of wakes they leave behind as they propagate and how this may be observed in cosmic microwave background (CMB) as temperature anisotropies via 21cm observations.

3.1 Formation via spontaneous symmetry breaking

Now for the purposes of this paper we shift our focus to 1D topological defects relating to the fundamental group $\pi_1(M)$ of the vacuum manifold, known as cosmic strings. These are formed from an inflationary phase transition in early universe between recombination and reheating, and their signal persists to our current time due to these defects being invariant under continuous deformations. Cosmic strings are of particular interest as their mass energy density μ is quadratically proportional to the energy symmetry breaking scale

η and thus allows us to probe particle physics models at very high energy scales relevant to structure formation [12].

To model cosmic strings, we consider an Abelian theory where we take the G-bundle to be a principal U(1)-bundle, meaning we no longer have to trace over the symmetry group generators and so we replace $\mathrm{tr}(F \wedge \star F)$ with $F \wedge \star F$ in the action, and drop the spinor terms in equation 1.1. Furthermore, we consider only the potential which depends uniquely on the massless scalar field which is given by $V(\phi)$. With this we can write a simplified action of this theory with a U(1)-phase symmetry $\phi \to e^{i\beta}\phi$ as:

$$S = -\frac{1}{2}\int F \wedge \star F + \int d^4y \left[\frac{1}{2}(D\phi)^2 - V(\phi)\right] \tag{3.1}$$

Here the scalar potential is a *symmetry breaking* potential which takes the form $V(\phi) = \frac{1}{4}g(\phi^*\phi - \eta^2)^2$, where g is the interaction coupling constant and η is the symmetry breaking (energy) scale. What's special about this potential is that when the system is above a critical temperature $T_c \sim \eta$ we have a symmetric state with a global minima but below this critical temperature this minima becomes a local maxima, meaning it is a *false* vacuum. This makes the scalar field take a metastable antisymmetric state [13] and the false vacuum decays via bubble nucleation. As the system cools below the critical temperature and undergoes a phase transition, spontaneous symmetry breaking occurs whereby the system obtains a symmetry not shared by its ground state, implying a degeneracy in the vacuum observable $\langle\phi\rangle$. The resulting potential is known as the *Goldstone* potential and has the following shape:

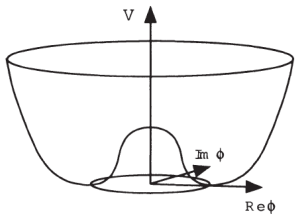

Figure 3. Visualization of the symmetry breaking Goldstone potential $V(\phi)$ which forms after cooling the system past the critical temperature T_c. The potential is defined over the complex scalar field plane (also known as the parameter space of the field) and its minima, i.e. the vacuum manifold, is a circle $M \simeq S^1$ [11].

Using the framework of finite-temperature field theory, it can be derived that the potential obtains a finite temperature correction during the phase transition in the form of:

$$\delta V_T = \frac{1}{2}\bar{g}T^2|\phi|^2, \tag{3.2}$$

where $\bar{g}$ is the interaction coupling constant rescaled to absorb boundary conditions on the variance of the scalar field, and T is the temperature of the system. The analogue to this correction in a quantum field theory would be finite loop-order corrections from

the interactions of spin-0 bosons. The degenerate vacua along the vacuum manifold S^1 are labelled by a phase angle α and the scalar field observable is given by [13]:

$$\langle \phi \rangle = e^{i\alpha}\eta/\sqrt{2} \tag{3.3}$$

During the decay of the false vacuum, four bubbles[†] of positive surface tension nucleate and their intersection form a point of energy in space [14]. By argument of continuity, we require the scalar field to vanish within the closure of the vacuum manifold S^1 [15]. At center of the circle, known as the *core*, the field has to go through a central hump in the potential and has a potential energy of the order $\mathcal{O}(T_c^4)$. The energy outside this core point quickly dissipates as the universe expands and so the energy is trapped within this point [11]. Moreover, in theories such as the Abelian-Higgs model, we can have string configurations which are translationally invariant, and thus this trapped energy occurs for points immediately above and below the core. Connecting these points gives use a line of trapped potential energy: the cosmic string topological defect. The process of forming topological defects when a system is drive through a continuous phase transition at a finite rate is known as the Kibble-Zurek mechanism [16]. The dynamics of these strings are given by the Nambu-Goto action for bosonic strings in string theory, but unlike bosonic string excitations in string theory, they don't end on branes and cosmic string loops cannot be excited to produce fields. Cosmic strings don't have ends and don't break, thus they either occur in nature as infinite length strings (bounded by the event horizon of our expanding universe), or as finite loops.

Cosmic strings are of interest as they possibly have significant effects on large-scale density distributions and anisotropies in the CMB. Furthermore, we can contract the energy mass density with Newton's gravitational constant to get a dimensionless quantity $G\mu$ known as the string *tension*, which will be crucial in cosmological observations and computing upper limits at high energy scales. In the following section we look at some conditions on the distribution and size of the strings based on a toy model of scalar fields.

3.2 Correlation lengths in spacetime

An important condition on the distribution of cosmic strings comes from its *correlation length* which characterizes how correlated the phases of the cosmic strings are given separation in spacetime. The formation of such topological defects A useful analogous model for computing the correlation length between cosmic string phases would be a toy model of a scalar field [6]. In this model we have a lattice of points where at each site a rod is confined to a plane and is pivoted off the vertical axis by some angle of ϕ. The rods have degrees of freedom that allows them to rotate and oscillate, and their tips are connected to one another via springs. The kinetic spring term in their action is analogous to the exterior covariant derivative term $(D\phi)^2$ in the cosmic string action. Furthermore, the potential for the system $V(\phi)$ is modelled via Newtonian gravity with the angle $\phi \in [0, \pi/2]$ being bounded by the first quadrant of the complex ϕ plane. Using these constraints, this model

[†]The nucleated bubbles themselves are domain wall topological defects which occur for non-trivial zeroth degree homotopy groups of the vacuum manifold: $\pi_0(M) \neq \mathbb{1}$.

is analogous to the scalar field model with the interaction potential $V(\phi) = \frac{1}{4}g(\phi^*\phi - \eta^2)^2$. If we heat the system such that its temperature T is much greater than the critical temperature $T_c \sim \eta$, all rods undergo large amplitude and high frequency oscillations. Given a large enough separation, their phases of oscillation become uncorrelated and this critical length beyond which there lacks correlation is known as the *correlation length* ξ. It follows by causality that there is an upper bound on the correlation length of the cosmic strings which is given by [6]:

$$\xi(t_c) < t_c, \tag{3.4}$$

where t_c is the causal horizon length at the critical temperature T_c (recall that we are using natural units). Analogously for the case of cosmic strings in spacetime, the boundaries between correlated phases become 2D topological defects (domain walls) and thus after a phase transition we will have a network of wall defects with mean separation of $\xi(t) \leq t$, for some horizon length t. Within these separated networks are cosmic strings with strongly correlated phases, and this tells us that there are no correlations on scales larger than t can be established, giving us a causal upper bound of the size of the network separations. Additionally, these correlation lengths can be interpreted as the mean curvature radius of string loops and separation lengths of long strings. Thus far we have information on the stability conditions of the cosmic strings, as well as the conditions on their correlation lengths past which they are uncorrelated. However, what about cosmic strings that are formed in loops? What distribution of loops is found after a phase transition in the early universe? We look at this in the following section and describe how cosmic string loops form in the first place.

3.3 Formation of cosmic string loops

Recall that in the previous section with the use of a toy scalar field model, a phase transition in the early universe produces a network of long cosmic strings which persist with a separation length of $\xi(t)$. Cosmic string *loops*, however, with radii equal to the correlation length will form after the phase transition via the intersection of two infinite length cosmic strings by exchanging ends. Alternatively, a long cosmic string can have part of itself form into a loop via self intersection and is visualized in the following figure:

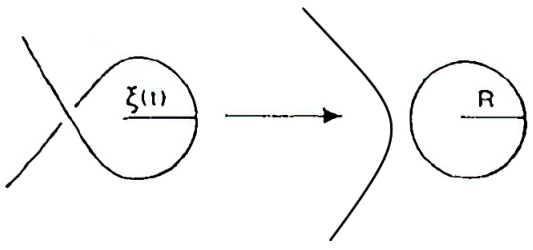

Figure 4. Visualization of the formation of cosmic string loops via self intersection [6]. The radius of curvature of the string before self intersection is given by its correlation length $\xi(t)$, which then becomes the radius R of the formed string loop.

When formed, the cosmic string loops shrink via oscillation due to their string tension and they decay gradually via gravitational radiation [6]. This means that their signal vanishes with time after forming from a phase transition in the early universe. Furthermore, it can be shown that as a consequence of the radius of curvature of the loops, the correlation length of the string loop network is proportional to its causality limit:

$$\xi(t) \sim t. \tag{3.5}$$

From this estimate (as well as the upper limit estimate for long string networks) it can be concluded that the fraction of the energy density of the total cosmic string network $\rho_\infty(t)$ to the background energy density $\rho_b(t)$ is fixed and in fact is proportional to the string tension [6]:

$$\frac{\rho_\infty(t)}{\rho_b(t)} \sim G\mu. \tag{3.6}$$

We see from above that the cosmic string network approaches what is known as a *scaling solution* in which the statistical properties of the networks are independent of time if all distances are scaled to the horizon distance t (alternatively known as the Hubble length l). Alternatively, this can be interpreted as the distribution of cosmic strings being *scale invariant* due to the rate at which cosmic strings form loops and lose energy. From this it suffices in our model of cosmic string signals to populate a single cosmic string per Hubble volume t^3. In the following section we outline the precise signal of the cosmic string to be detected which are temperature anisotropies in the CMB due to the wakes that the strings leave behind when propagating in spacetime.

3.4 CMB anisotropies via cosmic string wakes

As cosmic strings propagate relativistically through spacetime, — which contains local densities of plasma — much like boats in the sea they create *wakes* which give rise to velocity perturbations. Being that the string has uniform tension and length energy density, a gravitational lensing effect causes a conical structure to form in the space transverse to the string [17]. We can unwrap this cone onto the plane parallel to the string and we are left with the *deficit angle* of which the wake spans. The velocity perturbations coming from the cosmic string wake can be observed in string's rest frame whereby the ambient plasma moves towards the back of the wake. This process is depicted in the following figure:

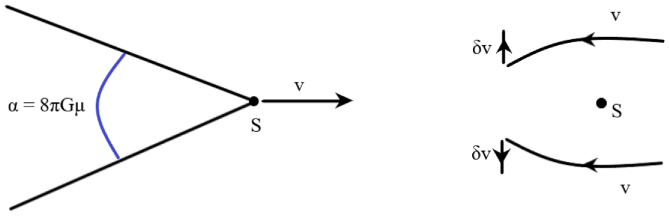

Figure 5. Visualization of a wake being formed in the plasma behind the string S. The left subfigure shows the string wake propagating at some velocity v with the width of the wake given by the deficit angle α. The right subfigure shows the same process in the rest frame of the cosmic string where the velocity perturbations δv can be seen going towards the back of the wake [6].

The width of the wake is given by the deficit angle $\alpha = 8\pi G\mu$ where $G\mu$ is the dimensionless string tension. As the string moves through plasma or a bath of dark matter, the velocity perturbations it induces towards the back of the wake is given by:

$$\delta v = 4\pi G\mu v\gamma(v), \tag{3.7}$$

where v is the velocity of the string and $\gamma(v) = 1/\sqrt{1-v^2}$ is the associated relativistic gamma factor. The velocity perturbations cause increased local densities of plasma in the plane transverse to the string, known as *planar overdensities*, for times after the time of equal matter and radiation t_{eq}. Now, how exactly do we extract a signal of the cosmic string from its wake? The created wakes cause anisotropies to form in the cosmic microwave background temperature distribution. This is due to a Doppler shift which occurs as radiation passes through different sides of the wake and so a change in temperature occurs. This temperature variation is a direct consequence of the deficit angle and would be negligible otherwise for a vanishing value of α. The temperature variation coming from the Doppler shift is visualized in the following figure:

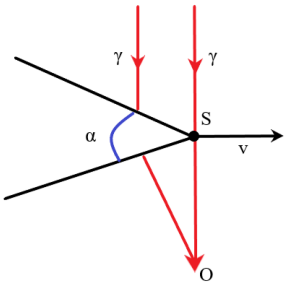

Figure 6. Visualization of CMB temperature anisotropy coming from the Doppler shift of radiation (red) passing on different sides of the cosmic string wake as a consequence of the deficit angle (blue). The resulting change in temperature is detected by an observer O [6].

Using finite temperature field theory, the temperature variation in the CMB caused by the process (normalized by the ambient temperature) is given by the following relation:

$$\frac{\delta T}{T} \sim 8\pi G\mu v\gamma(v). \tag{3.8}$$

We see that the normalized temperature anisotropy scales proportionally with the velocity of the string and so we expect to see stronger signals of strings moving at relativistic speeds. Now that we have conditions on the stability, distribution, and signal of the cosmic string, we move onto modelling it in redshift space (which we will later see if for convenience) where we can immerse it in primordial ΛCDM noise. From this we develop statistics to enhance and extract the signal of the cosmic string, as well as what the domain in which the string signal is bounded by is. The following section will delve into modelling cosmic strings of finite lengths along with an alternate mechanism of anisotropy in the CMB. Thereafter, we model the wake anisotropy signal in redshift space in Python and develop statistical methods to extract it.

4 String wake signals in redshift space

In this section we describe the network of cosmic string wakes using a finite length model and embed its topology in redshift space. We then develop statistics to extract its signal among spatial fluctuations from primordial ΛCDM noise and define the domain by which the signal is bounded.

4.1 Finite length wake model

For a network of cosmic strings we make use of the principal $U(1)$-bundle, consisting of the gauge group $U(1)$ over the Lorentzian 3+1D spacetime manifold $\mathcal{M}$. We can consider decomposing the spacetime by defining an equivalence relation over it, known as an *foliation*. This is the set of equivalence classes of its submanifolds — known as *leaves* of the foliation — which we select to be constant time slices, each indexed by the time coordinate t. These 3-dimensional spatial submanifolds, labelled as $\mathcal{M}_t$, are in fact *hypersurfaces* and within them the causal horizon distance is fixed by the index t. This tells us the correlation length estimate for the cosmic string network and and so the distance between correlated cosmic string phases (the interface of such correlations given by domain wall defects). Being that these submanifolds are 3-dimensional, this means that a set of cosmic strings will have correlated phases in some volume t^3. To make use of the scaling solution, we scale all distances to the causal horizon length and due to such only populate *one* cosmic string per Hubble volume t^3. For this to work, we move from a network of infinite length cosmic strings to a set of cosmic string segments of *finite length*. Each cosmic string segment which lives in separate Hubble volumes and their corresponding wakes have the following dimensions:

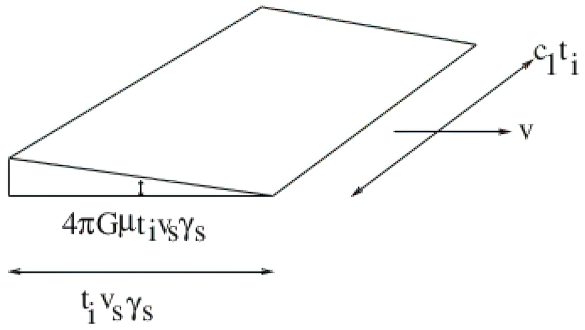

Figure 7. Visualization of a cosmic string wake immersed in the spatial submanifolds. These are bounded by the size of the Hubble volume and so are modelled with a finite length [18].

Here $c_1 \sim O(1)$ is a real constant of order unity, t_i is the time of formation (taken to be at recombination), v_s is the velocity of the string and γ_s is the associated relativistic gamma factor. The presence of this wake (which forms a wedge) causes distortions in temperature distributions and can be seen in anisotropies of the CMB map through 21 cm observations. As CMB radiation passes through the overdensities created by the wake, it is eventually emitted via the excitation of hydrogen within the wake [6] in quantized 21 cm packets. If the wake temperature emitted is colder than the ambient CMB photons coming from the surface of last scattering, then the wake absorbs the CMB radiation at 21 cm. If the wake temperature is hotter then it emits this 21 cm radiation. The string segments which are formed near recombination are the most numerous and thickest and so we focus on these set of strings. Although these segments will live for a Hubble time and decay (via the production of loops), the wake signal persists to present time. As light is emitted from the front and back of the wake (along the lightcone connecting the present time to the time of formation of the cosmic string), there is a frequency shift $\delta\nu$ between the two emitted rays [12]. This can be translated into a brightness temperature variation δT_b, and is the characterization of the cosmic string (wake) signal, given by [19]:

$$\delta T_b(\nu) = [0.07K]\frac{x_c}{1+x_c}\left(1-\frac{T_\gamma}{T_{K/g}}\right)\frac{\sqrt{1+z}}{2\sin^2\theta}. \tag{4.1}$$

Here x_c is the collision coefficient, T_γ is the temperature of the CMB photons prior to entering the gas cloud within the wake, $T_{K/g}$ is the kinetic temperature of the wake[†], z is the redshift, and θ is the angle off the line of sight from the observer to the wake. This gives us a wedge in physical space — the constant time hypersurfaces $\mathcal{M}_t$ — and within it a temperature gradient given by $\delta T_b(\nu)$. Moreover, from another analysis done [19], it is found that the wake signal is very narrow in the redshift direction. Thus, the cosmic string signal is characterized by a wedge temperature gradient in physical space, that is narrow in redshift space. This narrow feature will be useful in extracting the signal among

[†]The subscript is in reference if shock heating or incoherent gas thermal energy dominates, which changes the amplitude of the signal.

ambient fluctuations coming from primordial noise. In the following section we use this to immerse the wedge in redshift space and begin the construction of the wake in Python.

4.2 Implementation of wake signal

Now that we have laid the foundations for the signal of the cosmic string wake in physical space, we can begin its construction in Python for signal extraction. Consider a constant timeslice of the spacetime, given by $\mathcal{M}_t$, with a coordinate chart (x, y, z). In $\mathcal{M}_t$ we consider a Hubble volume t^3 centered at the origin of the physical coordinate system and within it we populate a single cosmic string wake (wedge). We construct the wake from six points following the dimensions given in the previous section. It is noted the deficit angle in all future figures is exaggerated to show the nature of the wake, which would otherwise look like a plane for actual values of the angle α. A wedge in physical space at some point coordinate within a Hubble volume (granted its boundary does not intersect the edges of the Hubble volume) will thus look like:

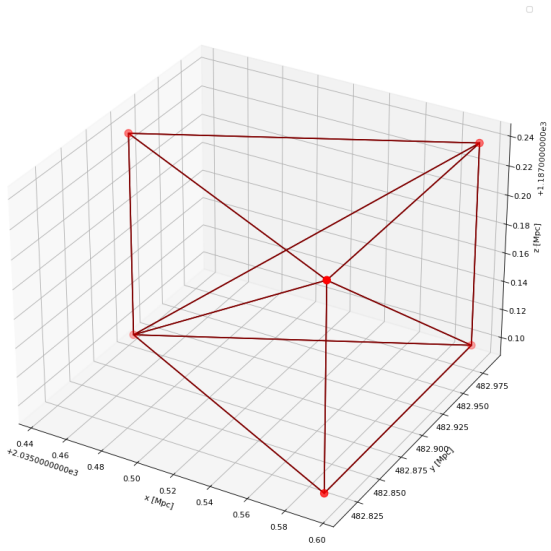

Figure 8. Visualisation of the cosmic string wedge in physical space bounded by the Hubble volume. The length scale of the axes are in Mpc.

Upon formation during recombination, the cosmic string wakes wont necessarily occur parallel to one of the axes of the coordinate system and so make the wake configuration more arbitrary we apply random rotations about all three axes via the generators of the $SO(3)$ group. Following this, due to the redshift dependence of the brightness temperature $\delta T_b(\nu)$, we would like for our vertical z-axis (in Mpc) to be rescaled to a dimensionless redshift axis, meaning we will work in *redshift space*. The scaling relation between distance and redshift is implicitly found from the non-linear ODE solutions to Einstein's equations using an FRW cosmology. The integral is non-elementary and is without an analytic solution, thus we proceed to generate the relationship numerically. This relation between the two looks like:

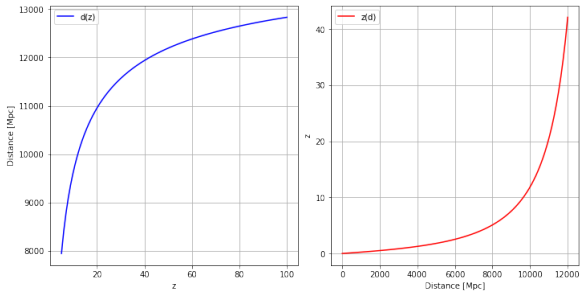

Figure 9. Scaling relationship between redshift and distance in Mpc for an FRW cosmology. The left subplot shows distance as a function of redshift, while the right subplot shows its inverse, redshift as a function of distance.

Using this we can rescale the vertical physical axis to a redshift axis. Finally, to model the wake in redshift space, we must take into account that in an expanding universe physical coordinates dilate. Thus, to match cosmological observations, we convert from physical coordinate to *comoving coordinates* via the relation on the cotangent bundle basis of the spacetime: $dx^{\mu}_{\text{phys}} = a(z)\ dx^{\mu}_{\text{com}}$. Here $a(z)$ is the redshift-dependent scaling factor for an expanding spacetime, dx^{μ}_{phys} is a differential form in the physical cotangent basis, and dx^{μ}_{com} is a differential form in the comoving cotangent basis. Using the scaling, dilation, and rotation transformations mentioned above, we have our construction for a wake in comoving-redshift space, which looks like:

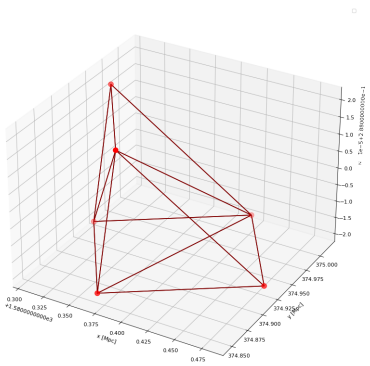

Figure 10. Visualization of the wake wedge in comoving-redshift coordinates for an arbitrary position and orientation.

Next, using complex convex hull sets, we can cover the wedge in simplices and test whether points lie within the hull. Using a flooding technique, we fill the Hubble volume with points and assign points within the wedge with the brightness temperature gradient $\delta T_b(\nu)$, which looks like:

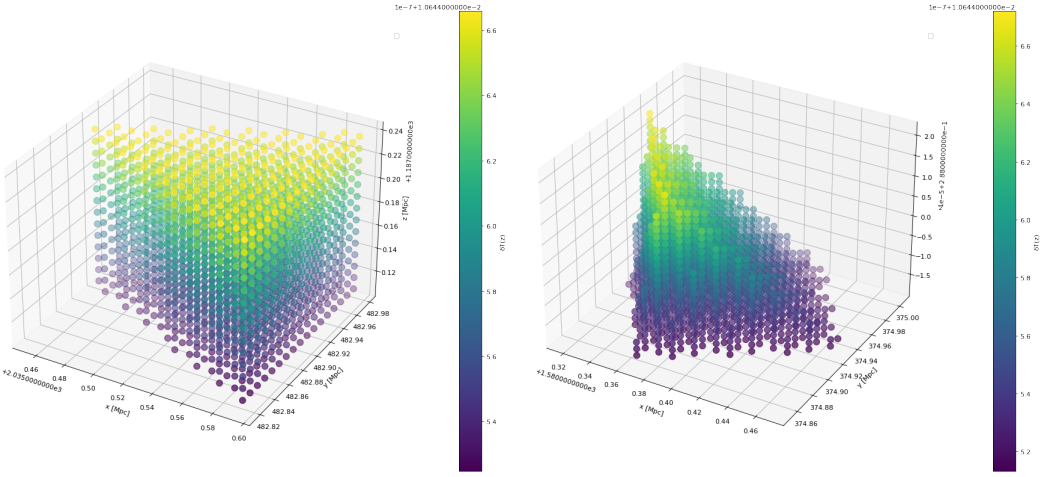

Figure 11. Visualization of points within the cosmic string wedge in comoving-redshift coordinates, each with an assigned brightness temperature value given by the function $\delta T_b(\nu)$. The left subfigure is for the wake without scaling, dilation, and rotation transformations. The right subfigure is the wake on the left after said transformations.

Now that we have our construction for the wake signal in comoving-redshift space as a convex hull set of points — each with a defined temperature given $\delta T_b(\nu)$ — we can move onto including the noisy background onsent by cosmological ΛCDM perturbations and look at statistics to extract the signal.

4.3 Signal extraction via match filtering maps

Before performing statistics which include a 3D noise map computed from simulations of early universe formation (which in covered in the following section), we first look at 2-dimensional case of immersing the wedge signal in a random noise map. This is to develop the methods which will be used when including accurate simulation noise in 3D space. The reduction to a 2D map is done via slices of the Hubble volume in $\mathcal{M}_t$. To visualize this slicing, consider the three following maps: a gradient map, a random noise map, and a line map. Each of them are 3D cubes within the Hubble volume with different temperature values on their surface. The gradient map has a temperature gradient on its surface (used to mimic the signal of the cosmic string wake), the noise map has a random distribution of temperature on its surface (used to mimic the primordial noise maps), and the line map is just a line of constant maximal temperature on the edge of the cube. If we consider a slice of these maps, we get the following figure:

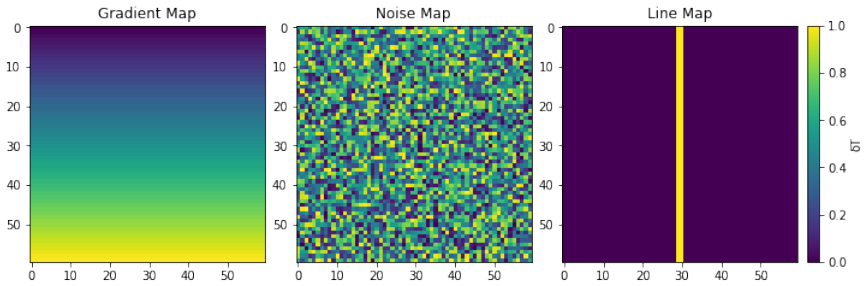

Figure 12. 2-dimensional slices along the vertical plane of example temperature maps along the vertical plane. The left map is the a slice of the gradient map used to model the wake, the middle is a a slice of a generic random noise map used to model the primordial fluctuations, and the right is an example of a map with a distinct line geometry used to elaborate the statistical framework which follows this figure.

If we superimposed these 2D maps, it would be very difficult to separate their individual signals and so we chose to *unfold* the maps to get a 1D string of information. To do so, we go along each row of the 2D map matrix (where each element of the matrix is a point on the map with a corresponding brightness temperature) and append the information of the individual points into a single array. We could also have done this process of unfolding by going along each column, which would give us a vertically unfolded array. The different directions of unfolding is important to take into account as it will modify the signal of the different maps. After unfolding the 2D maps above horizontally and vertically, we have the resulting figures:

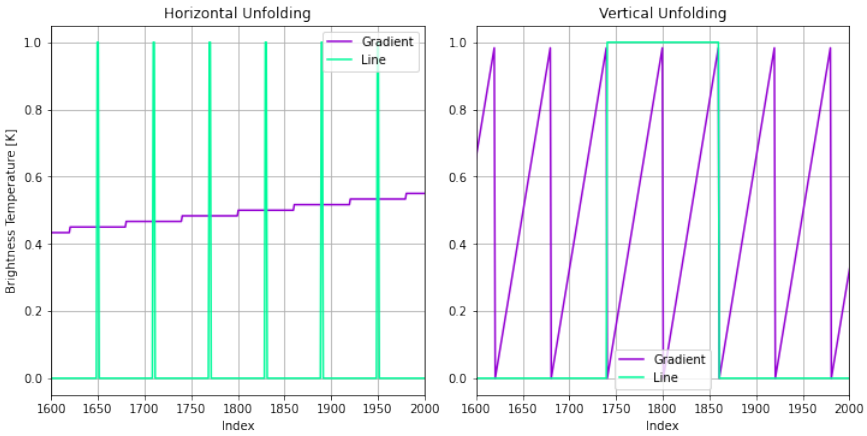

Figure 13. Unfolded temperature matrix of the gradient and line maps. The left subplot shows a horizontal unfolding where all the information of the 2D plot is unwrapped over some arbitrary index range. We see that the line signal appears periodic while the gradient wake signal steadily increases. The right subplot shows a vertical unfolding where the gradient signal is periodic and the line signal is a single bump.

We exclude the different unfoldings of the 2D noise map and the structure unfolded noise arrays are both equally chaotic and nothing is learned by them. We see that if

we reduce the information of the 2D noise maps to a 1D array we can see the signal of the individual maps, which change with the unfolding orientation. With this we can superimpose the 2D maps and unfold them to extract the individual signals (the gradient and line signals being obscured by the noise map) with the use of *match filtering* statistics. Since we unfolded a 2D matrix, we can use the 1D definition of match filtering given by [18]:

$$s(t) = \sum_{k=-n^2/2}^{n^2/2} h[t-k] \times d[k], \tag{4.2}$$

where s is the match filter amplitude for some index t which tells us if there is a signal in the array we input, h the array of the signal we wish to extract (in our case will be the wake gradient map in a vacuum), and d is the data array which is the wake gradient map immersed in the noise map. Here we see match filtering is simply a discrete convolution which sums up the values at different index separations, which is a statistic that is particularly good at maximizing the signal to noise ratio. The match filter amplitude is a tool used to see if given a data set in the form of an array contains signals that aren't just random fluctuations coming from noise. Using the definition of match filtering above, we compute the match filters for the different data samples in different unfolding orientations:

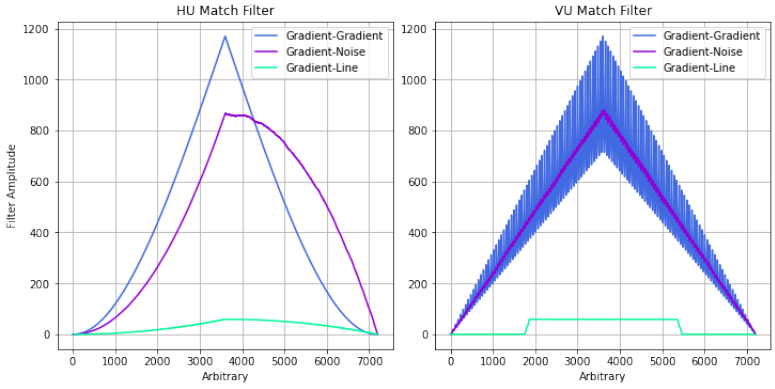

Figure 14. 1D match filtering for different data maps in various unfolding orientations. The left subplot shows the result of a match filter between different example maps after they are horizontally unfolded. The right subplot shows the result of a match filter between different example maps after they are vertically unfolded.

What does this mean? Consider the Gradient-Gradient curve in the left subplot. This curve tells us if given an array of the unfolded gradient map, what are the chances it is a gradient map? Being that the chance is 100%, we end up with a peak in the match filter. This is the ideal case where we look for the wake in a vacuum and find it. The Gradient-Noise curve tells us if given an array of the gradient map obscured by noise, what are the chances of finding the wake signal? We see that the resulting curve is still a peak and does indeed tell us there is a cosmic string wake signal within the noise. Finally, the Gradient-Line curve, this tells us the chances of finding a gradient map from a line map, which is very minimal. The right subplot is the same but for a vertical unfolding. In both

cases, we see observation of a wake in a background noise will have an amplitude that is bounded by the blue and purple curves; the blue curve is the case where the wake is in a vacuum and the magenta curve is the wake in noise.

Now what if we never unfolded the maps to begin with and just used a 2D match filter on the example maps? To do so we generalize the match filter definition in equation 4.2 to include matrices and are left with the following output:

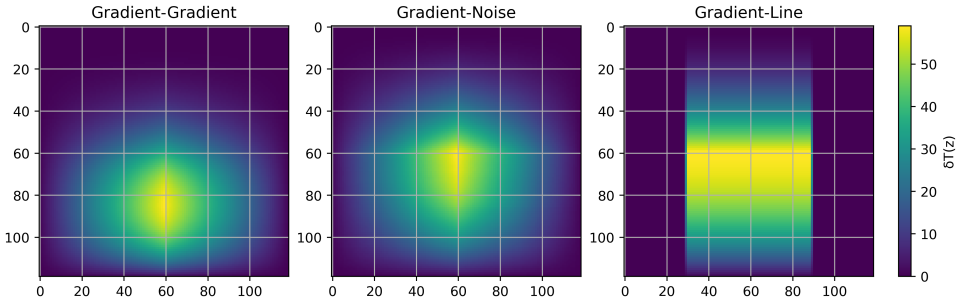

Figure 15. 2D match filtering for different data maps.

As can be seen above, the difference between the pure gradient-gradient match filter with the gradient-noise match filter is more nuance than the 1D case. This might not seem like the case, and so to elaborate this point further, we can unfold the 2D array *after* computing the 2D match filter in different orientations and compare the amplitudes. This results in the following figure:

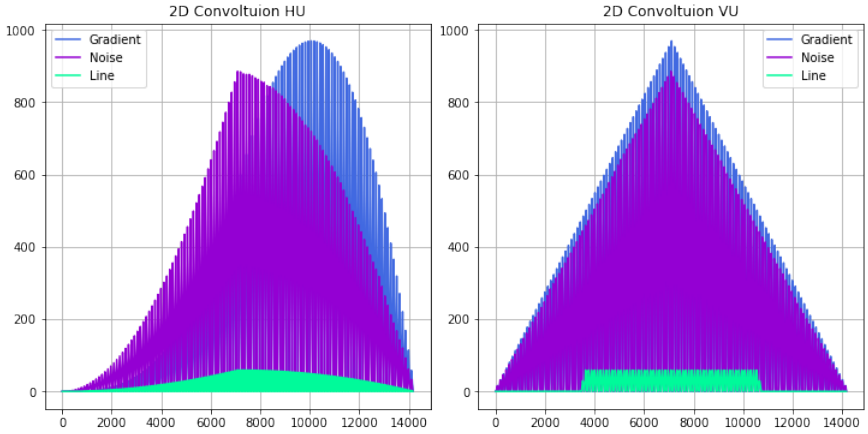

Figure 16. 2D match filter array for different data maps which is unfolded in different orientations. The left plot is for a match filter matrix that has been unfolded horizontally while the right plot is for vertical unfolding.

As can be seen above the cosmic string signal is again bounded by the blue and magenta curves, although this time their difference is much smaller than the 1D case. This makes it more difficult to confirm if a cosmic string wake is detected in a given data set map, and so we will proceed with 1D match filtering. To get some sense of what the actual cosmic

string wake signal will look like using 2D slices of its convex temperature hull, we use the 1D match filter between the string wake in physical-redshift space with the random noise map (normalized between 0 and 1), to produce the following plot:

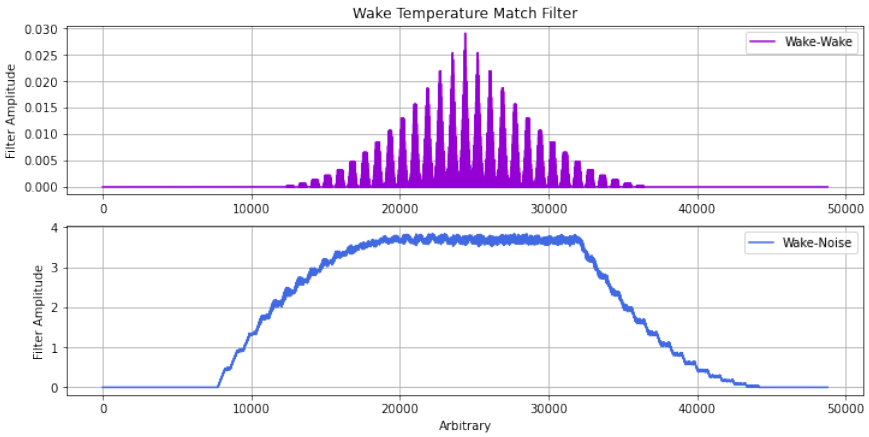

Figure 17. 1D match filtering using the information of the actual string wake gradient map. The top subfigure is the string wake gradient map convolved with itself while the bottom figure is the string map convolved with the string map immersed in random noise.

As can be seen above, there is a large difference is amplitude between the amplitudes of the match filter between a pure string gradient to string gradient filter versus a filter of a string map with a string map obscured by noise. Now that we have developed the formalism to extract the string signal obscured by noise, in the following section we move onto including the full 3D information of the cosmic string gradient map, as well as the 3D primordial ΛCDM noise map.

4.4 Match filtering along lines of sight

Now, we utilize the full 3-dimensional information of the cosmic string signal (with tension $G\mu \sim 3 \times 10^{-7}$), as well as the primordial noise occurring in the early universe. We begin by superimposing the 3D wake signal map with the 3D ΛCDM noise map to perform match filters along different slices of $\mathcal{M}_t$. First, we consider a ΛCDM noise map for a $200 \times 200 \times 200$ Mpc comoving box that is computed through 21cmFAST, a package used for computing cosmological simulations of physical fields in the early universe [20]. Furthermore, to match the size of our wedge map with the noise map, we choose a $29 \times 29 \times 29$ Mpc section of the larger comoving box. Within this noise map, for each redshift we may slice along the xy-plane to consider different lines of sight, and perform statistics on each slice. For the sake of demonstration we consider the 9th, 10th, and 11th slice of the 29 Mpc slices (respectively at redshifts 1,2,3). The slices for the 3D noise maps look like the following:

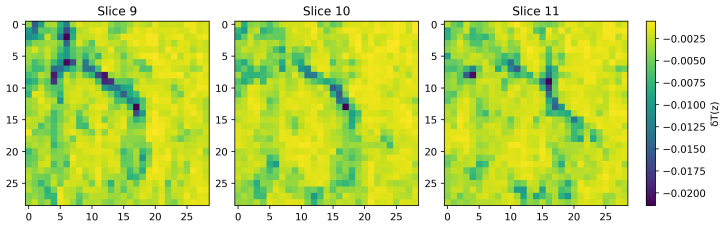

Figure 18. Line of sight slices of the ΛCDM primordial noise map, with dimensions of 29×29 Mpc.

Moreover, we can also pick the same index slices for our wake map, which looks like the following:

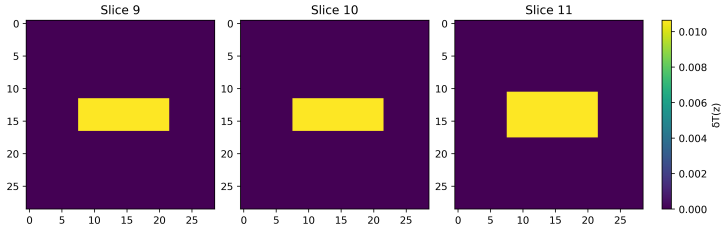

Figure 19. Line of sight slices of the string wake temperature map, with dimensions 29×29 Mpc. It is noted due to the small length scale, the temperature of the wake appears to be uniform in temperature but there are in fact small temperature variations given by the brightness temperature $\delta T_b(\nu)$. These will be our model parameters h which we convolve other maps with, as seen in equation 4.2.

Finally, we can superimpose the signal map of the cosmic string wake with the primordial noise map to get the following line of sight slices:

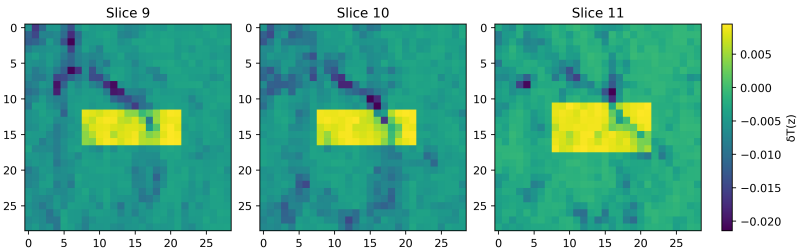

Figure 20. Line of sight slices of the combined string wake temperature and ΛCDM cosmological perturbation maps, with dimensions 29×29 Mpc.

From the above figure, we can see that at the string tension we are considering ($G\mu \sim 3 \times 10^{-7}$), the string signal is visible by eye. The match filter statistics are thus useful when modulating the string tension, and the signal to noise ratio becomes suppressed, meaning it can no longer be seen by looking at the signal map embedded in noise. As before we perform match filtering convolutions to extract the signal from the combined maps. The following plots are the result of 2D match filters between the different maps:

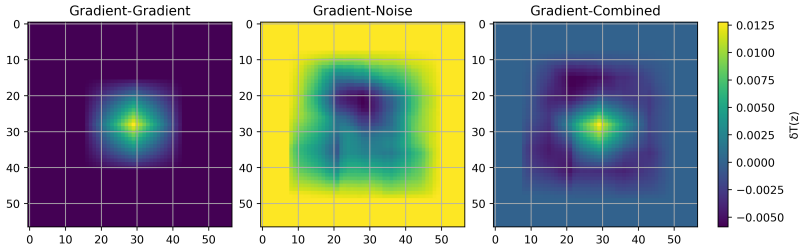

Figure 21. Result of 2D match filters of the different maps. The left most subplot is the result of a match filter between the gradient map with itself, the middle subplot is the wake signal convolved with the noise map, and the right most plot is the wake signal convolved wake signal map obscured by noise.

As can be seen from above, the match filter between the wake map and the wake map obscured by noise creates a peak within the 2D parameter space near the center where the wake is located. This shows us directly what the wake signal looks like if we are looking for a cosmic string signal in space. To get precise information on the domain which bounds the cosmic string signal (when including primordial noise), we unfold these match filter maps into a 1D array and plot the temperatures. This looks like the following figure:

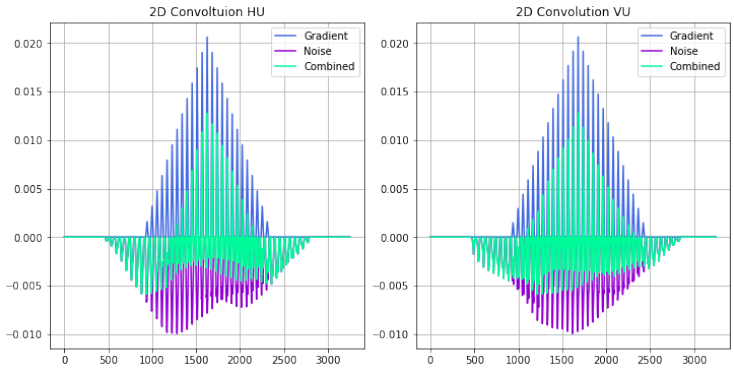

Figure 22. Unfolding of the 2D match filter maps. The different curves represent the unfolded match filter amplitude between the wake signal map and the various other maps. The left subplot if for a horizontal unfolding of the 2D match filter maps, while the right subplot is for a vertical unfolding.

We see that the signal of a string wake in a vacuum is has the most prominent peak in blue, closely followed by the signal of a string wake in a noisy background in green. This means we expect the signal of a string wake in cosmological observations to be bounded by the blue and green curves. Explicitly, the domain of the string signal (meaning the different values of the match filter amplitude which bounds it) would be between 0.0125 and 0.025, in both unfolding orientations. We can have a larger bounding domain if we unfold the noise and wake maps before performing a match filter. Consider unfolding the two maps before performing a math filter, which looks like the following:

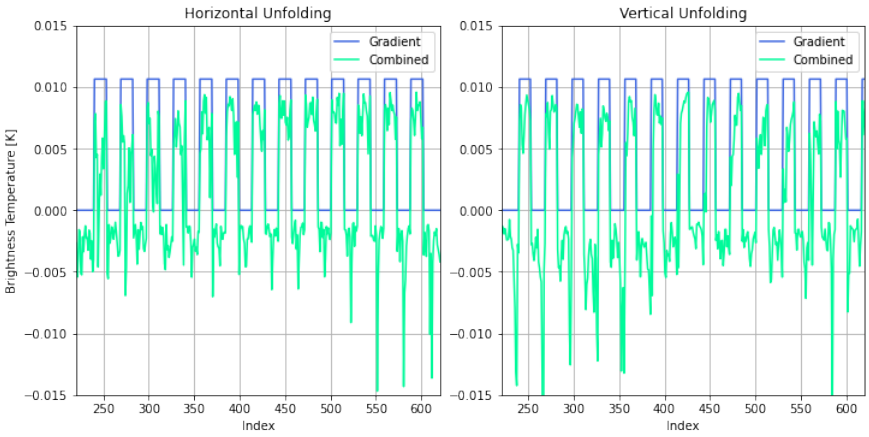

Figure 23. Unfolding of the 2D wake gradient map and the wake gradient map obscured by noise. The left subplot is a horizontal unfolding of the maps while the right subplot is for a vertical unfolding.

With the preceding unfolded maps, we can perform a 1D match filter to test the signal of the wake either in a vacuum or noisy background. The result of the 1D match filter is visualized in the following figure:

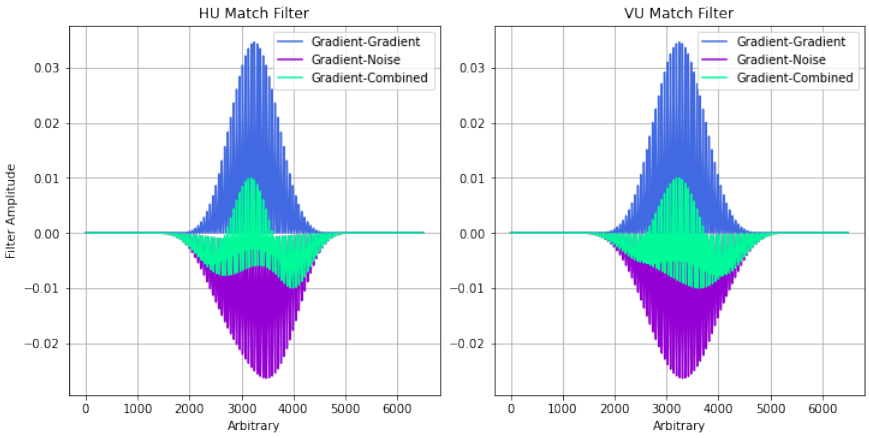

Figure 24. Results of the 1D match filters after having been first unfolded. The different curves represent the match filter amplitude between the wake signal map and the various other maps. The left subplot if for a horizontal unfolding of the 2D match filter maps, while the right subplot is for a vertical unfolding.

As can be seen from above, the signal of the wake in a vacuum has a much higher amplitude compared to the noise as in the 2D case. The difference between the amplitudes of a wake signal in a vacuum versus its signal in noise is much more prominent had we convolved the original 2D maps before unfolding them. Explicitly, the domain of the string signal in this case is between 0.010 and 0.035, in both unfolding orientations. This demonstrates a model in which we can employ statistics to able to extract the cosmic string wake signal from a noisy cosmological perturbation background map.

5 Caveats

It is worth mentioning some caveats of the analysis done above. First, the method in which points are detected within the wake is done using complex convex hulls. This algorithm becomes problematic when the blown up deficit angle is replaced by its actual value of $\alpha = 8\pi G\mu$ which is very small and thus the wake becomes a plane. The algorithm is based on connecting simplices along different vertices and does not work when the topology of the object is in 1D. Next, when converting from physical to comoving coordinates, one uses an inverse scaling factor of the form $a^{-1}(z) = (1-z)/z$, which can also be substituted for $a^{-1}(t_0) \sim 10^3$ for current observations. This scaling relation becomes an issue when wanting to scale physical axes to redshift axes using the numerical function from the *astropy* Python package, which doesn't converge for small or values of redshift, respectively given by the orders $\mathcal{O}(1)$ and $\mathcal{O}(1000)$. Thus, we are left with to work in a snapshot of physical coordinates to substitute for a continuous comoving coordinate system.

6 Conclusion

In this paper we developed a model and algorithm for extracting the signal of a U(1) topological defect (cosmic string) within a noisy cosmological perturbation background. We focused our attention to cosmic strings and looked at the construction of their wake in physical-redshift space. We developed statistics for extracting the cosmic string signal from a noisy background using match filtering, a convolutional statistic which maximizes the signal to noise ratio. It is found in the regime $G\mu \sim 3 \times 10^{-7}$ that a 1D match filter after unfolding the temperature matrix into an array shows a clear indication for what a string signal observation looks like. We also demonstrate the domain in which the string signal is bounded by. It is from this we conclude that given a data sample we know what domain to look for the cosmic string signal and how to extract it from fluctuation noise.

Acknowledgments

I would like to thank my supervisor Robert Brandenberger for his insights and guidance on the paper, as well as Mattéo Blamart for providing the primordial noise maps via universe simulations in 21cmFAST. Additionally, I'd also like to thank Oscar Hernández and his student Hans Hopkins for our discussions related to cosmic strings and inflationary cosmology. This was funded under the NSERC USRA award provided by the Natural Sciences and Engineering Research Council of Canada and the FRQNT scholarship supplement provided by the Fonds de Recherche du Québec Nature et technologies.

References

[1] N.D. Mermin, *The topological theory of defects in ordered media*, *Reviews of Modern Physics* **51** (1979) 591.

[2] N. Carqueville, C. Meusburger and G. Schaumann, *3-dimensional defect TQFTs and their tricategories*, *Advances in Mathematics* **364** (2020) 107024.

[3] M.E. Peskin, *An Introduction To Quantum Field Theory*, CRC Press (May, 2018), 10.1201/9780429503559.

[4] J. Baez and J.P. Muniain, *Gauge Fields, Knots and Gravity*, World Scientific (Oct., 1994), 10.1142/2324.

[5] H. Georgi and S.L. Glashow, *Unity of all elementary-particle forces*, *Physical Review Letters* **32** (1974) 438.

[6] R. Brandenberger, *Topological defects and structure formation*, *International Journal of Modern Physics A* **09** (1994) 2117.

[7] R. Brown, P.J. Higgins and R. Sivera, *Nonabelian Algebraic Topology*, EMS Press (Aug., 2011), 10.4171/083.

[8] A. Hatcher, *Algebraic Topology*, Cambridge University Press, Cambridge, England (Dec., 2001).

[9] J. Wess and B. Zumino, *Consequences of anomalous ward identities*, *Physics Letters B* **37** (1971) 95.

[10] E. Witten, *Global aspects of current algebra*, *Nuclear Physics B* **223** (1983) 422.

[11] T.W.B. Kibble, *Classification of topological defects and their relevance to cosmology and elsewhere*, *NATO Sci. Ser. C* **549** (2000) 7.

[12] R.H. Brandenberger, *Searching for Cosmic Strings in New Observational Windows*, *Nucl. Phys. B Proc. Suppl.* **246-247** (2014) 45 [1301.2856].

[13] T.W.B. Kibble, *Symmetry breaking and defects*, in *NATO Advanced Study Institute and COSLAB School: Patterns of Symmetry Breaking*, 11, 2002 [cond-mat/0211110].

[14] T.W.B. Kibble, *Topology of Cosmic Domains and Strings*, *J. Phys. A* **9** (1976) 1387.

[15] P.H. Frampton, *Consequences of vacuum instability in quantum field theory*, *Physical Review D* **15** (1977) 2922.

[16] B. Damski, *The simplest quantum model supporting the kibble-zurek mechanism of topological defect production: Landau-zener transitions from a new perspective*, *Physical Review Letters* **95** (2005) .

[17] A. Vilenkin, *Gravitational field of vacuum domain walls and strings*, *Physical Review D* **23** (1981) 852.

[18] M. Blamart, H. Fronenberg and R. Brandenberger, *Signal of cosmic strings in cross-correlation of 21-cm redshift and CMB polarization maps*, *JCAP* **11** (2022) 012 [2205.02725].

[19] D. Maibach, R. Brandenberger, D. Crichton and A. Refregier, *Extracting the signal of cosmic string wakes from 21-cm observations*, *Phys. Rev. D* **104** (2021) 123535 [2107.07289].

[20] S. Murray, B. Greig, A. Mesinger, J. Muñoz, Y. Qin, J. Park et al., *21cmfast v3: A python-integrated c code for generating 3d realizations of the cosmic 21cm signal.*, *Journal of Open Source Software* **5** (2020) 2582.